Linking structure and dynamics with two-neutron halos

Jesús Casal[1,*], *Mario* Gómez-Ramos[1], and *Antonio M.* Moro[1]

[1]Dpto. de Física Atómica, Molecular y Nuclear, Facultad de Física, Universidad de Sevilla, Apartado 1065, E-41080 Sevilla, Spain

Abstract. We present a theoretical description of (p, pn) reactions induced by two-neutron halo nuclei at intermediate energies. For this purpose, we use a reaction framework that incorporates a full three-body model for the projectile, and we focus on the cases of ^{11}Li and ^{14}Be. Our results provide a direct link between the structure properties of these nuclei and different reaction observables, such as relative-energy spectra or momentum distributions. We discuss also on the link between dineutron correlations and opening-angle distributions.

1 Introduction

Two-neutron halo nuclei are very exotic systems characterized by a diffuse matter distribution arising from the very weakly bound nature of two valence neutrons around a more compact core [1–3]. These (core + n + n) systems are called Borromean, i.e., they contain no bound binary subsystems and thus present a signature three-body structure [4, 5]. Typical examples are ^{6}He, ^{11}Li or ^{14}Be. Many different techniques have been used to explore the properties of two-neutron halo nuclei, such as Coulomb Dissociation [6, 7], neutron removal [8, 9], or low-energy scattering [10, 11], which provide invaluable insight into the limits of nuclear stabilily. Recently, two-neutron halo nuclei have been studied via quasifree knockout reactions with proton targets. The analysis of the relative-energy spectrum and momentum distributions after one-neutron removal provide information about the halo properties and the spectrum of the corresponding unbound subsystems [12–14]. Even more recently, the opening angle as a function of the intrinsic neutron momentum has been also studied to characterize dineutron correlations in the halo [15].

Three-body models are a well-established approach to describe two-neutron halo nuclei and have shown that, while a good knowledge of the unbound core + n subsystems is key to understand their properties, the correlation between the valence neutrons plays also a fundamental role [16, 17]. In this contribution, we provide a summary of some recent developments in the description of (p, pn) reactions induced by two-neutron halos using a full three-body model for the projectile. We first study the relative-energy spectrum and transverse momentum distributions at intermediate energies using the Transfer to the Continuum reaction framework [18]. Then, we adopt a sudden model approximation to analyze momentum and angular distributions, and we link the reaction observables with structure properties such as the partial-wave content and dineutron correlations.

*e-mail: jcasal@us.es

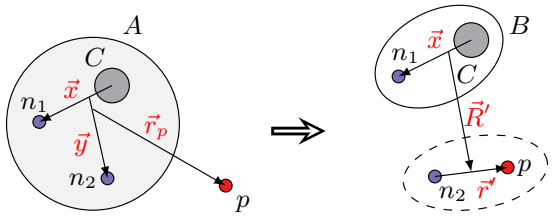

Figure 1. Schematic representation of the (p, pn) process induced by a two-neutron halo projectile.

2 Theoretical description

2.1 Three-body model and structure overlaps

Two-neutron halo nuclei can be described within the hyperspherical formalism [4]. In this work, as in Refs. [14, 19], we need the ground-state wave function of the Borromean projectile, $\Phi_{g.s.}(\boldsymbol{x}, \boldsymbol{y})$. Here, $\{\boldsymbol{x}, \boldsymbol{y}\}$ are the usual Jacobi coordinates (see Fig. 1). In order to build this state, we diagonalize the three-body Hamiltonian in a discrete basis, a procedure which is referred to in the literature as a pseudostate method. This method provides not only the ground state but also a discrete representation of the continuum (i.e., the pseudostates), but for the present calculations only the former is required. Different bases can be used, but we employ an analytical transformed harmonic oscillator basis [20]. Details about the three-body formalism can be found, for instance, in Ref. [21] and references therein.

The description of the knockout process requires the evaluation of a transition matrix involving both the ground-state of the three-body projectile and the scattering states, $\phi(\boldsymbol{k}_x, \boldsymbol{x})$, of the unbound core + n subsystem after the removal of a halo neutron (k_x is the intrinsic momentum). If the transition operator does not change the state of this residue, then the key structure ingredient for reaction calculations is the corresponding overlap

$$\varphi(k_x, \boldsymbol{y}) = \langle \phi(\boldsymbol{k}_x, \boldsymbol{x}) | \Phi_{g.s.}(\boldsymbol{x}, \boldsymbol{y}) \rangle_x, \qquad (1)$$

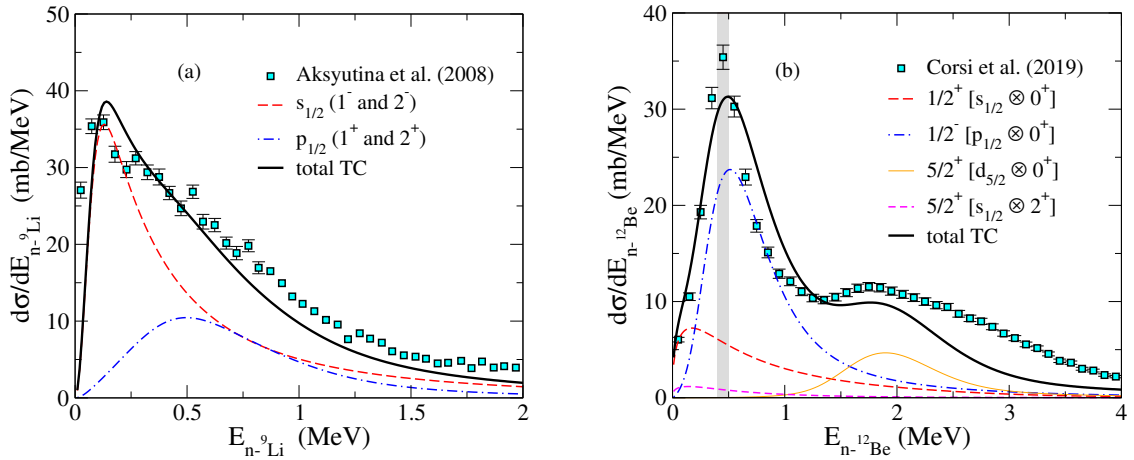

Figure 2. Relative-energy spectra of a) ^{10}Li and b) ^{13}Be after one-neutron knockout from ^{11}Li and ^{13}Be, respectively, and compared with the data of Refs. [12, 14] after convolution with the experimental resolution. The shaded area in the right panel is the region integrated to generate the momentum distribution in Fig. 3.

which can be split into different single-particle configurations of the knocked-out neutron using the appropriate coupling scheme for $\Phi_{g.s.}$ and ϕ [19, 22].

2.2 Reaction framework

We described the (p, pn) process within the Transfer to the Continuum (TC) framework. Using the structure overlaps defined above, the transition amplitude in prior form can be written as

$$\mathcal{T} = \sqrt{2}\langle \Upsilon_f^{(-)}(\boldsymbol{R}', \boldsymbol{r}')|V_{pn} + U_{pB} - U_{pA}|\varphi(k_x, \boldsymbol{y})\chi_{pA}^{(+)}\rangle, \quad (2)$$

where χ_{pA} is the distorted wave generated by the auxiliary optical potential U_{pA}, and $\Upsilon_f^{(-)}$ is the $B + p + n$ wave function in the final state, with B the unbound core + n residue. This expression assumes a participant-spectator approximation, in which the transition operator does not change the state of B, and the factor $\sqrt{2}$ arises from the two identical neutrons in the halo. To solve this problem, in the TC approach the final wave functions $\Upsilon_f^{(-)}$ are expanded in p-n continuum states following the binning procedure employed in the continuum-discretized coupled-channels method [23]. The dependence of the T-matrix on the momentum k_x of the binary subsystem after knockout enables the description of the corresponding relative-energy spectrum. Note that the TC method provides absolute cross sections, so no arbitrary scaling is needed to compare with (p, pn) experimental data.

3 Results

Recently, we carried out calculations to describe the ^{11}Li$(p, pn)^{10}$Li and ^{14}Be$(p, pn)^{13}$Be reactions [14, 19]. By adopting different structure models for the core + n unbound nucleus, we explored the sensitivity of the relative-energy spectrum after knockout to the position of resonances and virtual states in these subsystems, as well as to the resulting partial-wave content in the two-neutron halo wave function. In the case of ^{14}Be, our structure model included the coupling to the first 2^+ excited state of the ^{12}Be core, and we also analyzed the transverse momentum distributions. Here we summarize and compare some of these results. In Fig. 2, we show the ^{9}Li-n (left panel) and ^{12}Be-n (right panel) relative-energy spectra obtained within our reaction model at 280 MeV/nucleon and 265 MeV/nucleon, respectively, and compared with the data of Refs. [12, 14].

For ^{10}Li, our model includes the finite $(3/2^-)$ spin of the ^{9}Li core, so that the single-particle configurations $s_{1/2}$ and $p_{1/2}$ appear as doublets. For simplicity, here we present the summed contributions. As can be seen in the figure, the experimental data are consistent with parity inversion in ^{10}Li, with the $s_{1/2}$ contribution (coming mostly from a virtual state) being lower in energy than the $p_{1/2}$ resonances. The agreement with the data is remarkable, especially since no fitting is performed. Our three-body model for ^{11}Li is governed by s-wave components, with the p-waves contributing only about $\sim 31\%$ of the norm. Note that the same structure model has been also successful in describing ^{11}Li(p, d) transfer data [22].

The results for ^{13}Be are shown in the right panel of Fig. 2. In this case, the presence of core excitations in ^{14}Be leads to components in which the knocked-out neutron has a different angular momentum than the neutron than remains unperturbed in ^{13}Be. This is the case of the $5/2^+$ $[s_{1/2} \otimes 2^+]$ contribution, which corresponds to an $s_{1/2}$ single-particle component coupled to the 2^+ state of the core, but leading to a $d_{5/2}$ knockout. More details are given in Ref. [14]. As can be seen in the figure, our calculations are compatible with the spectrum being governed by a $p_{1/2}$ resonance around 0.5 MeV. This state carries about 60% of the ground-state norm. The agreement at low ^{13}Be energies is reasonable, while the calculations tend to underestimate the data at higher energies. This may be due to some missing components (or ^{13}Be resonances) in the wave function. Note that the ^{14}Be model used here does not include the excitation to all bound states of the ^{12}Be

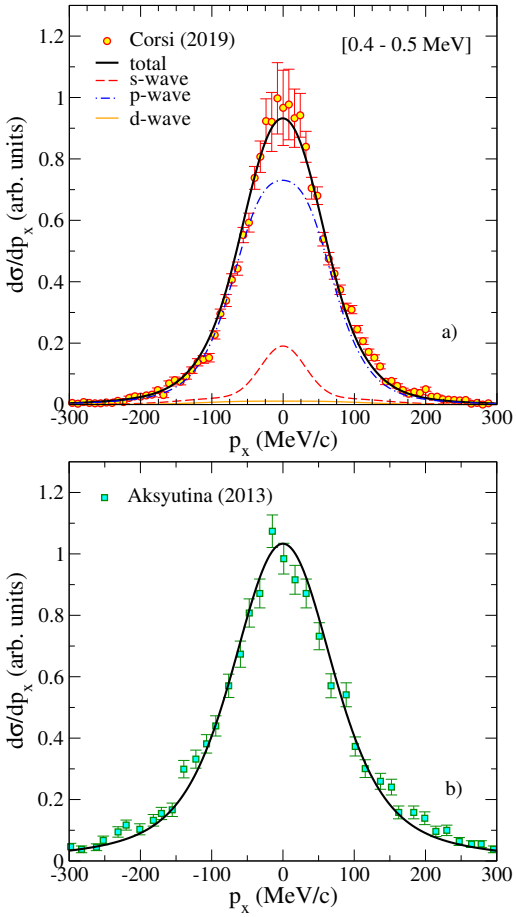

Figure 3. a) Transverse momentum distribution of the knocked-out neutron in the ^{14}Be$(p, pn)^{13}$Be reaction at 265 MeV/nucleon [14]. The ^{13}Be energy range (0.4-0.5 MeV) corresponds to the shaded area in Fig. 2, right panel. Calculations have been convoluted with the experimental resolution. b) The same but for the reaction at 304 MeV/nucleon [13, 25].

core, which will require further developments in the three-body description of the projectile.

The nature of the low-lying peak in the ^{13}Be spectrum has been long debated. In Ref. [24], the analysis of (p, pn) data at 69 MeV/nucleon was also interpreted with the population of a p-wave resonance. In the measurement of Refs. [13, 25] at 304 MeV/nucleon, however, the relative-energy spectrum could be described with a dominant s-wave. As we discussed in Ref. [14], our p-wave resonance is also consistent with the observed transverse momentum distributions. This is shown in Fig. 3 (top panel), integrated in the energy region corresponding to the shaded area in Fig. 2. The relative weights of s, p and d waves are given by the relative-energy spectrum, and the total distribution is rescaled to match the data through a χ^2 fit. It is clear from Fig. 3 that the width of the momentum distribution of Ref. [14] is totally compatible with a p-wave resonance. Interestingly, the same structure model and reaction calculations for ^{14}Be reproduce also the transverse momentum distribution for the (p, pn) data reported in Ref. [25], as shown in Fig. 3 (bottom panel). This highlights the consistency of the present results, which points

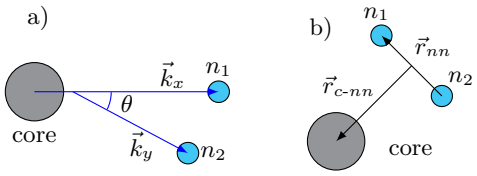

Figure 4. a) Momenta and opening angle in the Jacobi-Y representation; b) nn and core-nn distances in the Jacobi-T representation.

to a dominant p-wave contribution in the low-lying spectrum of ^{13}Be considering various (p, pn) observables.

3.1 Opening angle and dineutron correlations

In addition to exploring the properties of the unbound core + n subsystems, (p, pn) reactions with Borromean two-neutron halo nuclei can also be used to study dineutron correlations. This was proposed in Ref. [26] and realized experimentally in Ref. [15], where the measurement of the opening angle as a function of the intrinsic neutron momentum in ^{11}Li was linked to the surface localization of the dineutron. The mixing between different-parity components in the ground-state wave function favors dineutron correlations in coordinate space [27], thus leading to large opening angles (> 90 degrees) between the neutrons in momentum space.

The theoretical model in Ref. [26] assumes a quasi-free sudden approximation, where the reaction mechanism involves a zero-range V_{pn} interaction and absorption effects are given by the eikonal S-matrix between the proton target and the core of the Borromean nucleus. Within such model, the transition amplitude can be written as

$$\mathcal{T} \propto \langle \phi(\boldsymbol{k}_x, \boldsymbol{x}) \otimes e^{\boldsymbol{k}_y \cdot \boldsymbol{y}} | S(y) \Phi_{g.s.}(\boldsymbol{x}, \boldsymbol{y}) \rangle, \qquad (3)$$

where the S-matrix dependence on its impact parameter is approximated by the y coordinate (see Fig. 1). The previous equation involves the same structure overlaps introduced in Sec. 2.2 and can be seen as a distorted Fourier transform. By evaluating this transition amplitude, we can easily obtain the intrinsic momentum distributions in k_x, k_y and the opening angle between $\boldsymbol{k}_x$ and $\boldsymbol{k}_y$, in the so-called Jacobi-Y representation as depicted in Fig. 4 (left panel). Details on how to obtain the relevant expressions, as well as the absorption effects, will be presented elsewhere [28].

Here we restrict ourselves to the correspondence between dineutron correlation in coordinate space and opening angle in momentum space. In Fig. 5 (top panel), we present preliminary results for the the opening-angle distribution (integrated for all momenta) of ^{11}Li using the same three-body model introduced above. The result exhibits a clear asymmetry towards large angles ($\cos(\theta) < 0$). This is consistent with the recent experimental results in Ref. [15]. The large opening angle is linked to the spatial localization of the dineutron, which can be seen by plotting the two-dimensional ground-state density as a function of the nn and core-nn distances in the so-called Jacobi-T representation (see Fig. 4). This is also shown in Fig. 5

(bottom panel), where the probability density has a clear maximum at small r_{nn} distances, i.e., small angles between the neutrons in coordinate space. Calculations of the intrinsic momentum distributions and the average opening angle as a function of the intrinsic neutron momentum are in progress.

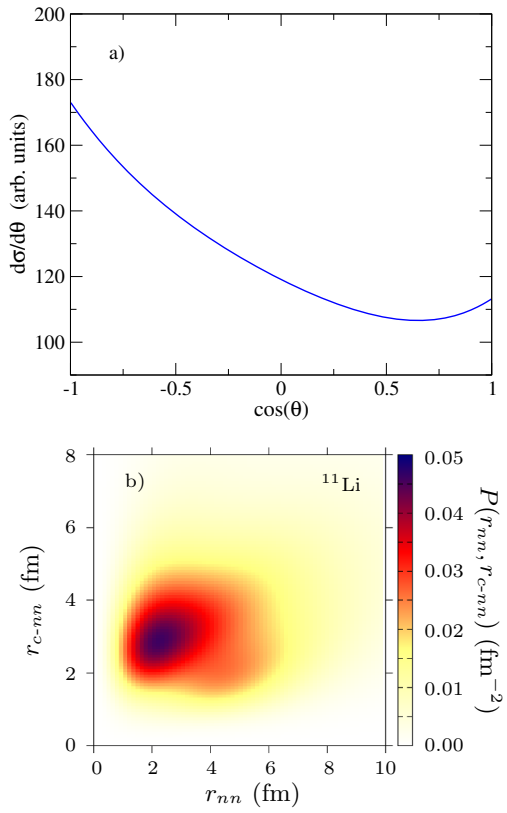

Figure 5. a) Opening angle distribution for the ^{11}Li(p, pn) reaction. b) Ground-state probability density of ^{11}Li as a function of r_{nn} and $r_{c\text{-}nn}$. Results are preliminary.

Acknowledgements

This work has been partially funded by the Spanish Ministerio de Ciencia, Innovación y Universidades (project No. FIS2017-88410-P), by the European Union research and innovation programme under Marie Skłodowska Curie Actions (grant agreement 101023609), and by the European Social Fund and Junta de Andalucía (PAIDI 2020, grant number DOC-01006).

References

[1] I. Tanihata *et al.*, Phys. Rev. Lett **55**, 2676 (1985)
[2] P. G. Hansen and B. Jonson, Europhys. Lett. **4**, 409 (1987)
[3] K. Riisager, Rev. Mod. Phys. **66**, 1105 (1994)
[4] M. V. Zhukov *et al.*, Phys. Rep. **231**, 151 (1993)
[5] E. Nielsen, D. Fedorov, A. Jensen, and E. Garrido, Phys. Rep. **347**, 373 (2001)
[6] T. Nakamura *et al.*, Phys. Rev. Lett. **96**, 252502 (2006)
[7] K. J. Cook *et al.*, Phys. Rev. Lett. **124**, 212503 (2020)
[8] H. Simon *et al.*, Phys. Rev. Lett. **83**, 496 (1999)
[9] H. Simon *et al.*, Nucl. Phys. A **791**, 267 (2007)
[10] L. Acosta *et al.*, Phys. Rev. C **84**, 044604 (2011)
[11] M. Cubero *et al.*, Phys. Rev. Lett. **109**, 262701 (2011)
[12] Y. Aksyutina *et al.*, Phys. Lett. B **666**, 430 (2008)
[13] Y. Aksyutina *et al.*, Phys. Lett. B **718**, 1309 (2013)
[14] A. Corsi *et al.*, Phys. Lett. B **797**, 134843 (2019)
[15] Y. Kubota *et al.*, Phys. Rev. Lett. **125**, 252501 (2020)
[16] K. Hagino and H. Sagawa, Phys. Rev. C **72**, 044321 (2005)
[17] J. Casal and E. Garrido, Phys. Rev. C. **102**, 051304(R) (2020)
[18] A. M. Moro, Phys. Rev. C. **92**, 044605 (2015)
[19] M. Gómez-Ramos, J. Casal, and A. M. Moro, Phys. Lett. B **772**, 115 (2027)
[20] J. Casal, M. Rodríguez-Gallardo and J. M. Arias, Phys. Rev. C **88**, 014327 (2013)
[21] J. Casal *et al.*, Phys. Rev. C **102**, 064627 (2020)
[22] J. Casal, M. Gómez-Ramos, and A. M. Moro, Phys. Lett. B **767**, 307 (2017)
[23] N. Austern *et al.*, Phys. Rep. **154**, 125 (1987)
[24] Y. Kondo *et al.*, Phys. Lett. B **690**, 245 (2010)
[25] Y. Aksyutina *et al.*, Phys. Rev. C **87**, 064316 (2013)
[26] Y. Kikuchi, K. Ogata, Y. Kubota, M. Sasano, and T. Uesaka, Prog. Theor. Exp. Phys. **2016**, 103D03 (2016)
[27] F. Catara, A. Insolia, E. Maglione, and A. Vitturi, Phys. Rev. C **29**, 1091 (1984)
[28] J. Casal and M. Gómez-Ramos, in preparation (2021).